RSC Advances

PAPER

View Article Online
View Journal | View Issue

Cite this: *RSC Adv.*, 2017, **7**, 1490

Removal of trace arsenic to below drinking water standards using a Mn–Fe binary oxide

Jiefei Li,[a] Hiroki Gyoten,[b] Akinari Sonoda,[c] Qi Feng[b] and Mei Xue*[a]

A series of Mn–Fe binary oxides with different Mn/Fe mole ratios were prepared by a co-precipitation method for the development of a high performance arsenic adsorbent from arsenic-contaminated drinking water. The Mn–Fe binary oxides and their arsenic adsorption reactions were characterized by X-ray powder diffraction, Fourier transform infrared spectroscopy, scanning electron microscopy, N_2 adsorption and inductively coupled plasma mass spectrometry. The As(III) and As(V) adsorption results reveal that the arsenic adsorption ability is strongly dependent on the Mn/Fe mole ratio and surface area of the adsorbent. The MF4/6-10(H_2O_2) sample which was prepared by alkaline solution containing H_2O_2 shows the excellent arsenic removal of 99.9%, reducing As(III) concentration from 2 mg g^{-1} to 2 μg L^{-1}, which can clear the new arsenic limit of 10 μg L^{-1} in drinking water by the WHO. Manganese species in the adsorbent accelerates oxidation of As(III) to As(V), which enhances the As(III) adsorption ability of the adsorbent. Meanwhile, iron species in the adsorbent have a role to form surface OH groups, which is an important factor for the effective adsorption of As(V) by a surface chelating reaction.

Received 15th November 2016
Accepted 1st December 2016

DOI: 10.1039/c6ra26806d

www.rsc.org/advances

Introduction

Common arsenic species in the environment include arsenate (As(V)), arsenite (As(III)), dimethylarsenic acid and monomethylarsenic acid. In natural water, arsenic presents primarily in inorganic forms which are more toxic than the organic forms.[1–3] Arsenic contamination in ground water is creating serious environmental problems. As(III), which is more toxic than As(V), is the dominant arsenic in ground water.[4–6] Long-term uptake of arsenic-contaminated drinking water has negative impacts on human health.[7,8] About 125 million people in Bangladesh have been estimated to be adversely affected by arsenic-contaminated drinking water.[9] In order to minimize these health risks, the WHO and the U.S. Environmental protection agency has revised the maximum contaminant level of arsenic in drinking water from 50 μg L^{-1} down to 10 μg L^{-1}, and this new limit of 10 μg L^{-1} has become effective since January 2006.[10]

Many methods such as coagulation/precipitation, ion exchange, membrane filtration, adsorption, reverse osmosis and electrocoagulation process had been used for arsenic removal.[11–17] In these methods, arsenic adsorption removal is considered to be one of the most promising technologies because it is effective in the removal of low-concentration arsenic from liquids.[16–21] Up to now, several adsorbents have been reported by some studies, and the results suggest that amorphous hydrous ferric oxide, poorly crystalline hydrous ferric oxide and goethite have high arsenic adsorption ability.[16,22] Gu *et al.* have prepared granular activated carbon-based iron-containing adsorbents in which the impregnated hydrous ferric oxide is amorphous form which could remove arsenic most efficiently.[23] Jang *et al.* have used hydrous ferric oxide incorporated into diatomite adsorbent for arsenic column application. The adsorbent shows higher arsenic adsorption ability and adsorption capacity compared to AAFS-50 adsorbent (activated alumina that is used as arsenic removal adsorbent in Bangladesh).[24,25] Oscarson *et al.* prepared Fe_2O_3-coated MnO_2 adsorbent to reduce As(III) concentration by oxidizing it to As(V) under adsorption conditions. MnO_2 (birnessite) is a very effective oxidant and it can oxidize the As(III) to As(V), while Fe_2O_3 cannot convert As(III) to As(V) within 72 h.[26] Above studies demonstrated that the iron oxide or/and manganese oxide have a strong affinity for arsenic adsorption. Recently, a series of Fe–Mn binary oxide with different Mn/Fe ratio were synthesized by co-precipitation method using potassium permanganate, iron sulfate heptahydrate and NaOH at pH of 7 and 8. As(III) oxidation and sorption are affected by Mn/Fe ratio of the binary oxide. The adsorbents with Mn/Fe ratio of 1 : 3 and 1 : 6 show maximum As(III) and As(V) uptake of 114 mg g^{-1} and 60 mg g^{-1}, respectively.[27] However, until now the optimum conditions for the preparation of Mn–Fe binary oxide adsorbents are unclear.

Herein, we report the preparation condition of a high performance Mn–Fe binary oxide adsorbent, and the influence of preparation conditions on its arsenic removal ability,

[a]*School of Chemistry and Chemical Engineering, Inner Mongolia University, 235 West University Road, Hohhot, 010021, China. E-mail: setsubai@sina.cn; Fax: +86-471-4992981*

[b]*Department of Advanced Materials Science, Faculty of Engineering, Kagawa University, 2217-20 Hayashi, Takamatsu, 761-0396, Japan*

[c]*Health Technology Research Center, National Institute of Advanced Industrial Science and Technology (AIST), 2217-14 Hayashi, Takamatsu, 761-0395, Japan*

including alkaline component and pH of reaction solutions, Mn/Fe mole ratio and calcination treatment conditions. After the optimization of preparation conditions, the As(III) concentration in drinking water can be reduced from 2 mg L^{-1} to 2 μg L^{-1} using this adsorbent.

Experimental

Preparation of adsorbents

Mn–Fe binary oxide was prepared by co-precipitation method. Manganese nitrate ($Mn(NO_3)_2$, 1 mol L^{-1}) and iron nitrate ($Fe(NO_3)_3$, 1 mol L^{-1}) solutions were mixed at a desired Mn/Fe mole ratio of 10/0, 8/2, 6/4, 4/6, 2/8, or 0/10 (total volume: 20 mL), and then deionized water was added to a final volume of 100 mL. Desired amount of NaOH was dissolved in 200 mL of water to make an alkaline solution. The alkaline solution was added into the metal nitrate solution under vigorously stirring condition, after which the stirring was continued for 5 min and aged for 12 h. The obtained suspension was separated and washed 3 times with deionized water by centrifugation (7000 rpm, 10 min) and dried at 40 °C. The adsorbents are designated as MF*X*-*Y*, where MF expresses Mn and Fe, *X* corresponds to the mole ratio of starting Mn/Fe mole ratio, and *Y* the pH value of the reacting solution.

Another series of Mn–Fe binary oxide was prepared using an alkaline solution (200 mL) containing 3% H_2O_2 (H_2O_2 acts as oxidizing agent). The preparation procedure was the same as above. The adsorbents obtained are designated as MF*X*-*Y*(H_2O_2), *etc.*, similar to those obtained without H_2O_2.

Low-crystalline akaganeite (β-FeOOH), high crystalline akaganeite, and schwertmannite were prepared for the comparison of their arsenic adsorption abilities. Low-crystalline akaganeite was obtained by the hydrolysis of $FeCl_3$ at pH = 10 and high-crystalline akaganeite by the hydrothermal treatment of urea-containing $FeCl_3$ solution at 100 °C.[28,29] Schwertmannite was prepared by hydrolysis of $FeCl_3$ in a solution containing Na_2SO_4 at 60 °C.[30]

Adsorption experiments

Adsorption experiments were performed by a batch method. All chemicals were of analytical grade and were purchased from Kanto Chemical Co., Inc. (Osaka, Japan). The As(III) and As(V) solutions were prepared by diluting arsenic standard solutions of 100 mg L^{-1} As(III) (As_2O_3 in 0.005% HCl solution) and 1000 mg L^{-1} As(V) (As_2O_5 in 0.0005% HCl solution) with ultrapure water, respectively. The arsenic adsorption from a diluted solution was carried out by adding the adsorbent (25 mg) into the As(III) or As(V) solution (100 mL) and stirring for 22 h at room temperature. After the arsenic adsorption, the arsenic concentration of the supernatant solution was analyzed using a Seiko inductively coupled plasma mass spectrometer (ICP-MS SPQ9000) in [As] < 2 mg L^{-1} concentration range, or a Seiko inductively coupled plasma atomic emission spectrometer (ICP-AES SPQ7800) in [As] ≧ 2 mg L^{-1} concentration range. Adsorption isotherm was obtained by using solutions containing 10–20 mg L^{-1} As(III) or As(V).

Characterization of adsorbent

The crystal phase of the adsorbent was characterized using a powder X-ray diffractometer (XRD) (Rigaku type RINT2100) with CuKα ($\lambda = 0.15418$ nm) radiation. BET surface area was calculated from a nitrogen adsorption isotherm (obtained on a Quantachrome-type 1-C apparatus) for adsorbent degassed at 120 °C for 2 h. The particle size and morphology of the adsorbent were observed using field-emission scanning electron microscopy (FE-SEM) (JEOL, JSM-6700FZ). Fourier transform infrared (FT-IR) spectra were obtained by KBr method on a Perkin-Elmer Infrared spectrometer (2000 series).

The Fe and Mn contents of the adsorbent were determined by ICP-AES spectrophotometry after the sample was dissolved in a 5 M HCl solution containing H_2O_2. The Mn valence in the adsorbent was determined by redox titration. An adsorbent (0.1 g) was dissolved in a mixed solution of $Na_2C_2O_4$ (0.150 mol L^{-1}, 10 mL), H_2SO_4 (20% v/v, 10 mL) and H_2O (100 mL), and heated at 70 °C. The concentration of residual $C_2O_4^{2-}$ ions was determined by titration with $KMnO_4$ (0.020 mol L^{-1}) at around 70 °C. The active oxygen content can be calculated by eqn (1)

$$\text{Active oxygen content (mmol g}^{-1}) = [C_{Na_2C_2O_4}V_{Na_2C_2O_4} - C_{KMnO_4}V_{KMnO_4} \times 5/2]/(2 \times W) \quad (1)$$

where *C*: concentration of $Na_2C_2O_4$ or $KMnO_4$ (mol L^{-1}), *V*: volume of $Na_2C_2O_4$ or $KMnO_4$ (mL), *W*: weight of adsorbent (g). The mean valence of Mn was calculated using the active oxygen content and Mn content.[31]

Result and discussions

Synthesis and characterization of Mn–Fe binary oxide adsorbent

Since Mn(II) ions precipitate effectively in a highly alkaline condition in the absence of oxidizing agent, we precipitated the binary oxides at pH 12, changing the starting Mn/Fe mole ratio (10/0, 8/2, 6/4, 4/6, 2/8 and 0/10). The synthesis conditions and composition analysis results of the adsorbents are shown in Table 1. The Mn/Fe mole ratios of the adsorbents well correlate with that of the starting solutions, suggesting that both Fe(III) and Mn(II) ions are effectively precipitated at pH 12. The Mn valence (Z_{Mn}) shows a unique tendency to increase with a decrease of Mn content. This result reveals that Fe(III) promotes the oxidation of Mn(II) to Mn(IV) in the co-precipitation reaction. The XRD patterns prepared adsorbents are shown in Fig. 1. A Mn_3O_4 phase (JCPDF 24-0734) is formed in a Mn/Fe mole ratio range of 10/0 to 6/4, and its crystallinity decreases with reducing Mn/Fe mole ratio. An α-FeOOH phase (JCPDF 29-0713) is formed at Mn/Fe = 0/10. At Mn/Fe = 2/8 and 4/6, the samples show XRD patterns of nearly amorphous phase. The XRD result suggests that these binary oxide samples are not a simple mixture of Mn_3O_4 and α-FeOOH crystals, but Mn and Fe are connected by a random network of Fe–O and Mn–O bonds to form amorphous phase.

These samples have large BET specific surface areas, and they keep the large surface areas even after heat treatment at 350 °C (Table 1). FE-SEM images of the adsorbents are shown in Fig. 2. Sample MF10/0-12 with Mn_3O_4 phase mainly consists of

Table 1 Preparation conditions and properties of Mn–Fe binary oxides prepared using NaOH solution at pH 12

	Preparation conditions		Properties of adsorbent				
Adsorbent	Mn/Fe mole ratio	Precipitation pH	Mn/Fe mole ratio	Z_{Mn}[a]	S_{BET}[b] ($m^2\ g^{-1}$)	Crystal phase	S_{BET} (350)[d] ($m^2\ g^{-1}$)
MF10/0-12	1	12	—	—	23	Mn_3O_4	15
MF8/2-12	4	12	4.18	3.01	136	Mn_3O_4	99
MF6/4-12	1.5	12	1.60	3.09	255	Mn_3O_4	161
MF4/6-12	0.67	12	0.71	3.39	277	Am[c]	189
MF2/8-12	0.25	12	0.30	3.74	275	Am	173
MF0/10-12	0	12	—	—	166	α-FeOOH	68

[a] Mean valence of manganese. [b] BET surface area. [c] Amorphous phase. [d] BET surface area after calcination at 350 °C.

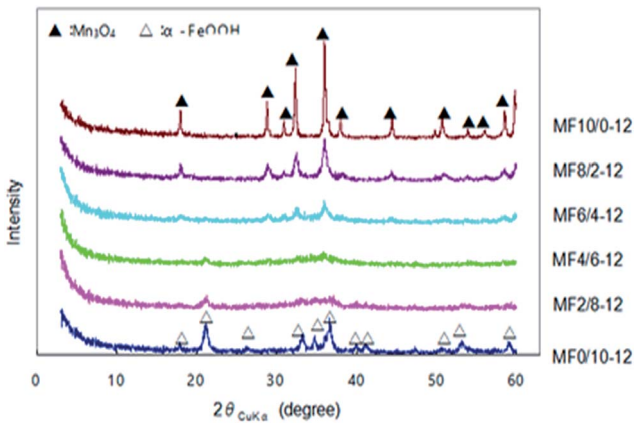

Fig. 1 XRD patterns of Mn–Fe binary oxides prepared by reacting Mn(II)–Fe(III) mixed solutions with different Mn/Fe mole ratios and NaOH solution at pH 12.

aggregates of particles with a size about 50 nm. It contains a small amount of fibrous particles. Sample MF0/10-12 with α-FeOOH phase consists of aggregates of rod-like particles. MF4/6-12 consists of particles with irregular shape and size, though most of the particles are not clearly observed due to its amorphous nature.

As(III) adsorption on Mn–Fe binary oxide adsorbents

A preliminary study of As(III) adsorption from a solution containing As(III) (20 mg L^{-1}) showed that the adsorption was fast enough to reach adsorption equilibrium by treatment for only 4 h. The As(III) removals by the adsorbents from a diluted solution containing 2 mg L^{-1} As(III) are shown in Table 2. All the adsorbents except for MF10/0-12 show good As(III) removals of above 99%. The MF6/4-12, MF4/6-12 and MF2/8-12 samples can reduce the As(III) concentration from 2 mg L^{-1} to 2 μg L^{-1}. After heat treatment at 350 °C, the amorphous and low-crystalline samples (MF6/4-12, MF4/6-12, MF2/8-12) keep good As(III) removals (above 95%), which is probably due to their large surface areas (Table 1).

The As(III) adsorptive ability of the Mn–Fe binary oxide adsorbents were compared with those of the conventional adsorbents. Three conventional iron oxide adsorbents, low- and high-crystalline akaganeite (β-FeOOH, JCPDF 34-1266) and low-crystalline schwertmannite ($Fe_8O_8(OH)_{8-2x}(SO_4)\cdot nH_2O$, JCPDF 47-1775) were prepared. The As(III) removals increased in the order schwertmannite (78.9%) < high crystalline β-FeOOH (90.2%) < low crystalline β-FeOOH (97.5%), which is in agreement with the results in the literature that low-crystalline β-FeOOH shows the highest arsenic removal.[32] The MF6/4-12, MF4/6-12 and MF2/8-12 samples show the excellent As(III) removals of 99.9% when compared with the conventional iron oxides adsorbents.

The As(III) and As(V) removals from a concentrated solution (60 mg As per L) were studied using three kinds of adsorbents (Table 2). It is noticeable that the As(III) removals are nearly equal to the As(V) removals. The arsenic uptake increases in the order MF10/0-12 < MF0/10-12 < MF4/6-12, which correlates well with the order of the surface areas of the adsorbents. These results suggest that the As(III) and As(V) ions are adsorbed on the surface of the binary oxide adsorbent.

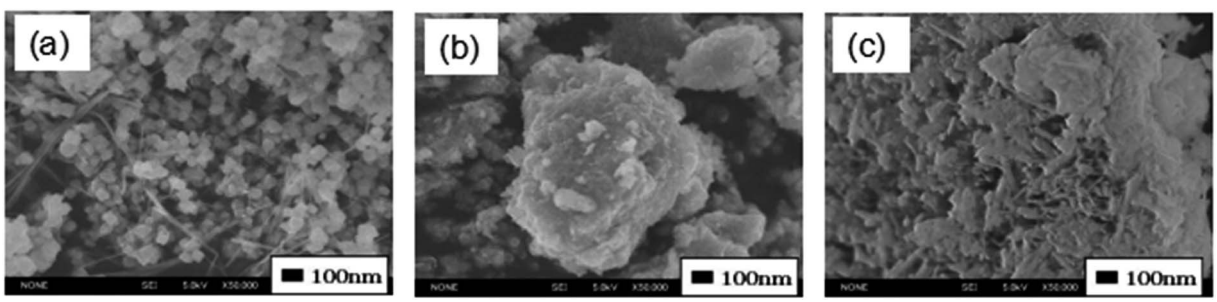

Fig. 2 SEM photographs of (a) MF10/0-12, (b) MF4/6-12 and (c) MF0/10-12 samples.

Table 2 Arsenic adsorption results for Mn–Fe binary adsorbents prepared using NaOH solution at pH 12

	As(III) removal from a diluted solution[a]				Arsenic removal from a concentrated solution[b]			
	Before calcination		After calcination at 350 °C		As(III)		As(V)	
Adsorbent	Removal (%)	Residual conc. (μg L^{-1})	Removal (%)	Residual conc. (μg L^{-1})	Removal (%)	Uptake (mg g^{-1})	Removal (%)	Uptake (mg g^{-1})
MF10/0-12	75.1	489	38.0	1240	22	13	5	3
MF8/2-12	99.9	2	81.9	362	—	—	—	—
MF6/4-12	99.9	2	98.3	34	—	—	—	—
MF4/6-12	99.9	2	96.4	72	87	52	77	46
MF2/8-12	99.8	5	97.5	51	—	—	—	—
MF0/10-12	99.6	28	28.0	165	70	42	60	36

[a] Adsorbent: 25 mg; solution: 100 mL; initial As(III) concentration: 2 mg L^{-1}; contact time: 22 h. [b] Adsorbent: 100 mg; solution: 100 mL; initial arsenic concentration: 60 mg L^{-1}; contact time: 22 h.

Kinetics study

Adsorption rate is an important parameter in terms of As removal efficiency. Kinetics study of As(III) adsorption on MF6/4-12 at an initial concentration of 100 ppb (100 μg L^{-1}) of arsenic stock solution has been investigated by a batch experiment. The process of As(III) removal is rapid and 5 min was required to remove 92%, and equilibrium is reached after 120 min. As(III) adsorption kinetics tests were carried out and two conventional kinetic models (pseudo-first-order and pseudo-second-order) were applied to analyse the experiment data.[15,33]

The pseudo-first-order model can be described as:

$$\ln(q_e - q_t) = \ln q_e - k_1 t \quad (2)$$

where q_e and q_t (μg g^{-1}) are the adsorbed As(III) amounts on at equilibrium and at various times t, respectively, and k_1 is the rate constant of the pseudo-first-order model of adsorption (min^{-1}), the values of q_e and k_1 can be determined from the intercept and slop of the linear plot of *versus* t.

The pseudo-second-order model can be described as:

$$\frac{t}{q_t} = \frac{1}{k_2 q_e^2} + \frac{t}{q_e} \quad (3)$$

where q_e and q_t are defined as in the above pseudo-second-order model and k_2 (g (μg min)$^{-1}$) is the rate constant of the pseudo-second-order model of adsorption, which can be obtained from the linear plot of t/q_t *versus* t.

Fig. 3 presents the result of kinetic studies. The corresponding kinetic parameters and correlation coefficients are summarized in Table 3. The pseudo-second-order model with the correlation coefficient R^2 of 1 is found to be more suitable for fitting the kinetic data than the pseudo-first-order model with the correlation coefficient R^2 of 0.9688, suggesting that the adsorption process might be chemisorptions. The experimental adsorption capacity is also in accordance with the calculated adsorption capacity obtained from the pseudo-second-order model.

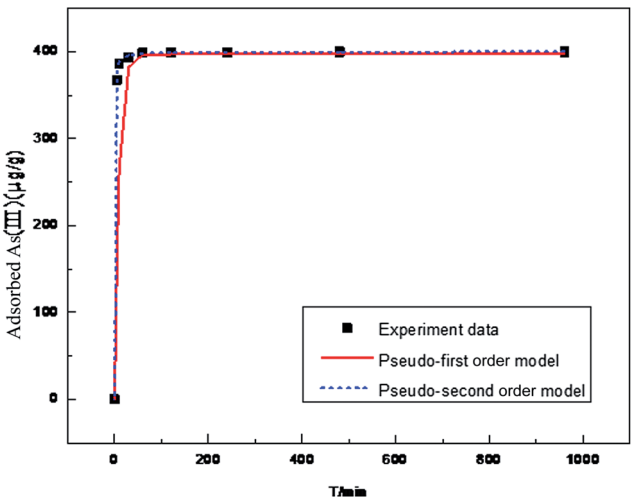

Fig. 3 Adsorption kinetics of As(III) on MF6/4-12 at room temperature (25 mg of MF6/4-12 in 100 mL of 100 ppb As(III) stock solution).

Dependence of arsenic removal on pH value of solution

The effect of solution pH on arsenic adsorptive behavior was studied using MF4/6-12. The adsorbent (25 mg) was added to As(III) or As(V) solution (2 mg L^{-1}, 100 mL) and stirred for 24 h at room temperature. The pH of arsenic solution was adjusted by HCl and NaOH solutions. The dependences of arsenic removals on the pH values of the solution are shown in Fig. 4. The removals at pH < 7.5 are nearly 100% with MF4/6-12 for both As(III) and As(V) and they decrease with increasing pH value in the region pH > 8. The similar trends with respect to pH suggest that parts of As(III) was oxidized to As(V) by this adsorbent. Zhang *et al.* reported that Fe–Mn binary oxide with Mn/Fe mole ratio of 1 : 3 showed As(V) removals of nearly 100% at pH < 5.5, and the removal decreased with increasing pH value in the region pH > 6.[27] Our study indicates that the MF4/6-12 should be more effective for the majority of water supplies, which normally have a pH range of 6.5–8.5.[34]

Lower pH is favorable for the protonation of adsorbent surface, which increases the positively charged sites on the adsorbent surface, and enlarges the attraction force between the positively charged adsorbent surface and As anions, thus increases the adsorption ability of the adsorption in the lower

Table 3 Kinetic parameters for the adsorption of As(III) by MF6/4-12[a]

	Pseudo-first-order model			Pseudo-second-order model		
q_e, exp. (μg g^{-1})	k_1 (min^{-1})	q_e, cal. (μg g^{-1})	R^2	k_2 (g μg^{-1} min^{-1})	q_e, cal. (μg g^{-1})	R^2
399.6	0.1097	396.9	0.9688	0.0089	400.0	1

[a] Adsorption kinetics of As(III) on MF6/4-12 at room temperature (25 mg of MF6/4-12 in 100 mL of 100 ppb As(III) stock solution).

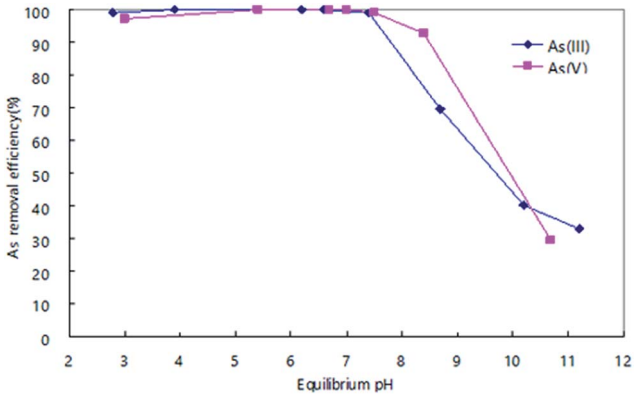

Fig. 4 Dependences of As(III) and As(V) removals on solution pH value by MF4/6-12 sample. Adsorbent: 25 mg; solution: 100 mL; concentration of As(III) or As(V): 2 mg L^{-1}; contact time: 24 h.

pH region. In higher pH region, the negatively charged sites are dominating on the adsorbent surface, which reduces adsorption ability of the As anions.[35,36]

Adsorption isotherms

Adsorption isotherms for As(III) and As(V) on MF4/6-12 are shown in Fig. 5. The curve fitting by non-linear least square method reveals that the experimental data fit Langmuir equation rather than Freundlich equation. The Langmuir equation is represented as:

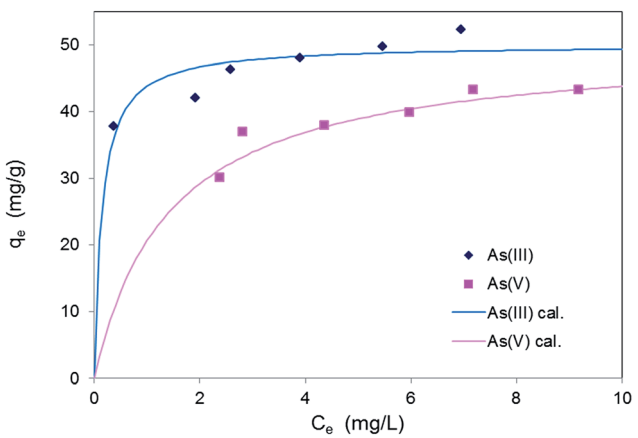

Fig. 5 Adsorption isotherms of As(III) and As(V) on MF4/6-12 sample. Adsorbent: 25 mg; solution: 100 mL; contact time: 24 h; initial As(III) concentration: 10–20 mg L^{-1} (pH 5.7); initial As(V) concentration: 10–20 mg L^{-1} (pH 4.4).

Table 4 Parameters of adsorption isotherm for arsenic adsorption on MF4/6-12[a]

	Langmuir model	
Adsorption species	q_m (mg g^{-1})	b (L mg^{-1})
As(III)	50	7
As(V)	50	0.7

[a] Adsorbent: 25 mg, solution: 100 mL, contact time: 22 h; initial As(III) concentration: 10–20 mg L^{-1} (pH 5.7); initial As(V) concentration: 10–20 mg L^{-1} (pH 4.4).

$$q_e = q_m b C_e/(1 + bC_e) \quad (4)$$

where C_e: equilibrium arsenic concentration (mg L^{-1}), q_e: equilibrium arsenic uptake (mg g^{-1}), q_m: saturation adsorption capacity of arsenic (mg g^{-1}), b: adsorption constant (L mg^{-1}). From the least square fitting of experimental data, the saturation adsorption capacities (q_m) were evaluated as 50 mg g^{-1} for both As(III) and As(V), and the adsorption constants (b) were evaluated as 7 and 0.7 L mg^{-1} for the As(III) and As(V) adsorptions, respectively (Table 4). Since the b value reflects the strength of adsorption, the larger b value for As(III) suggests that As(III) interact strongly with adsorbent compared with As(V), although the reason for the stronger adsorption of As(III) is not clear.

Effect of H_2O_2 on the composition of Mn–Fe binary oxide

It is well known that H_2O_2 accelerates the oxidation of Mn(II) during hydrolysis, which causes a rapid precipitation of

Table 5 As(III) adsorption results for Mn–Fe binary adsorbents prepared using NaOH solution containing H_2O_2 at different pH conditions[a]

Adsorbent	As(III) removal (%)	As(III) uptake (mg g^{-1})	Residual conc. (μg L^{-1})
MF6/4-6.4(H_2O_2)	99.8	8.0	5
MF6/4-9.7(H_2O_2)	99.9	8.0	2
MF6/4-12(H_2O_2)	71.0	5.7	581
MF10/0-10(H_2O_2)	35.0	2.8	1300
MF8/2-10(H_2O_2)	96.5	7.7	70
MF6/4-10(H_2O_2)	99.6	8.0	8
MF4/6-10(H_2O_2)	99.9	8.0	2
MF2/8-10(H_2O_2)	99.8	8.0	4
MF0/10-10(H_2O_2)	99.3	7.9	15

[a] Adsorbent: 25 mg; solution: 100 mL; initial As(III) concentration: 2 mg L^{-1}; contact time: 22 h.

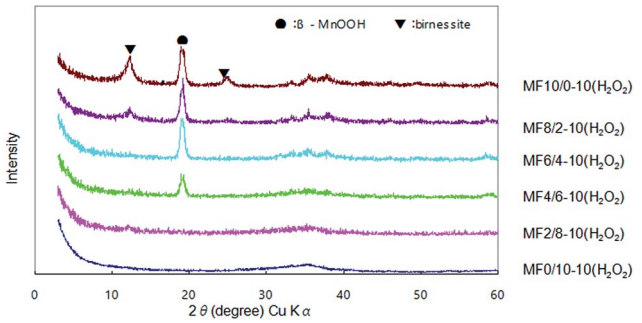

Fig. 6 XRD patterns of Mn–Fe binary oxides prepared by reacting Mn(II)–Fe(III) mixed solutions with different Mn/Fe mole ratios and NaOH solution containing H_2O_2 at pH 10.

manganese oxide. We studied the precipitation of Mn–Fe binary oxide using a NaOH solution containing H_2O_2. The As(III) removals by the adsorbents prepared using the NaOH solutions containing H_2O_2 are summarized in Table 5. The As(III) removal depends on the precipitation pH. It increases in the order MF6/4-12(H_2O_2) < MF6/4-6.4(H_2O_2) < MF6/4-9.7(H_2O_2) for samples precipitated at pH 12, 6.4, and 9.7, respectively. The suitable precipitation pH is around 10 under the H_2O_2 oxidation conditions.

Therefore, the binary oxides with different Mn/Fe mole ratios (10/0, 8/2, 6/4, 4/6, 2/8 and 0/10) were prepared at pH 10. The XRD patterns of the adsorbents are shown in Fig. 6. Sample MF10/0-10(H_2O_2) prepared from pure $Mn(NO_3)_2$ is a mixture of β-MnOOH (JCPDF 18-0804) and birnessite (JCPDF 23-1046). The content of birnessite phase decreases rapidly with increasing Fe content in the adsorbent, while β-MnOOH phase remains even with increasing Fe content to Mn/Fe = 4/6 (MF4/6-10(H_2O_2)). MF2/8-10(H_2O_2) and MF0/10-10(H_2O_2) samples are amorphous phase, which show a broad peak at around 35 degrees, suggesting the formation of ferrihydrite type iron hydroxide.[37]

Their As(III) adsorptive behaviors are similar to those prepared without H_2O_2 addition (Table 5). The MF10/0-10(H_2O_2) adsorbent without Fe addition exhibits low As(III) uptake, while the Mn–Fe binary oxide adsorbents exhibit considerably high As(III) uptakes. The MF4/6-10(H_2O_2) adsorbent exhibits the most

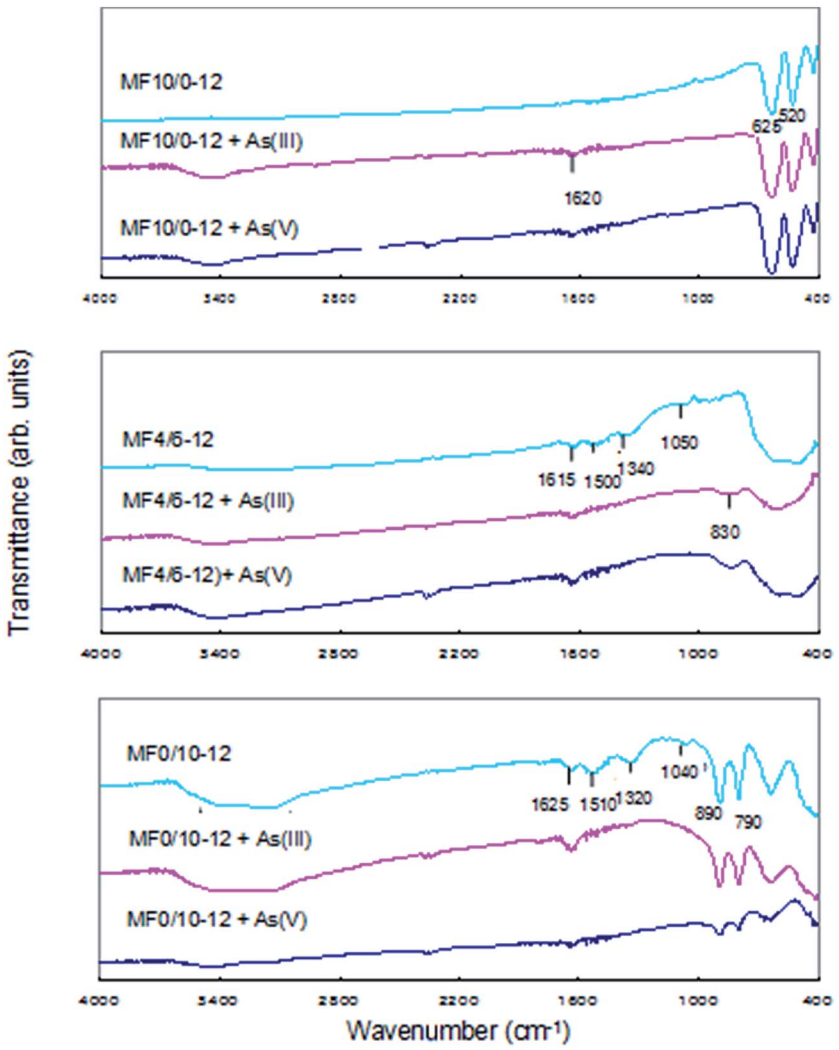

Fig. 7 FT-IR spectra of adsorbents before and after As(III) and As(V) adsorptions.

excellent As(III) removal ability, reducing As(III) concentration to 2 μg L^{-1}. The above results reveal that the Mn–Fe binary oxides of amorphous and low-crystalline phases have high arsenic removal ability from a diluted solution.

Mechanism of arsenic adsorption

In order to clarify the adsorption mechanism, the physical and chemical analyses were carried out on the MF10/0-12, MF4/6-12 and MF0/10-12 samples before and after As(III) and As(V) adsorptions. Adsorbents (100 mg) were added into an As(III) or As(V) solution (60 mg As per L, 100 mL) and stirred for 22 h at room temperature. The FT-IR spectra of the adsorbents before and after the arsenic adsorption are shown in Fig. 7. For MF0/10-12 with α-FeOOH phase, the vibration bands at 1040, 1320 and 1510 cm^{-1} corresponding to O–H bending vibration of FeO(OH) almost disappear by As(III) or As(V) adsorption. The bands at 890 and 790 cm^{-1}, which can be ascribed to the lattice vibration of α-FeOOH, are rarely changed by the arsenic adsorption. This result indicates that arsenic is bound to the surface OH group of α-FeOOH by a chelating reaction.[38] The bands (1500, 1340, and 1050 cm^{-1}) corresponding to the vibration of surface OH group are also observed in the spectrum of MF4/6-12 although it has amorphous phase but not α-FeOOH phase. The bands disappear by the arsenic adsorption, suggesting that the OH group on the surface of binary oxide involves the arsenic adsorption similar to the case of α-FeOOH. These bands are not observed in the spectrum of MF10/0-12 with Mn_3O_4 phase, whose FT-IR pattern does not change obviously by arsenic adsorption. The formation of OH group on the adsorbent surface is an important factor for the effective adsorption of arsenic.

The change in Mn valence after arsenic adsorption was investigated using MF4/6-12. The As(III) and As(V) uptakes are 52 and 46 mg As per g, respectively, as shown in Table 2. The Mn valence decreased significantly from 3.39 to 2.99 after As(III) adsorption, suggesting that oxidation of As(III) to As(V) took place during the adsorption, accompanied by the reduction of Mn(IV) to Mn(III). The decrease of Mn valence is small (from 3.39 to 3.27) in the case of As(V) adsorption. Moore *et al.* and Nesbitt *et al.* demonstrated that the oxidation of As(III) by the synthetic birnessite surface proceeds by two step pathway (reaction (5) and (6) as follows), involving the reduction of Mn(IV) to Mn(III) and then Mn(III) to Mn(II).[39,40]

$$2MnO_2 + H_3AsO_3 = 2MnOOH^* + H_3AsO_4 \quad (5)$$

$$2MnOOH^* + H_3AsO_3 + 4H^+ = 2Mn^{2+} + H_3AsO_4 + 3H_2O \quad (6)$$

We can conclude from the above results that the adsorption of As(III) on binary oxide progresses *via* the oxidation to As(V) followed by the chelating reaction with surface OH groups. Manganese species in the binary oxide accelerates the oxidation of As(III) to As(V). Since As(III) is adsorbed after oxidation to As(V), its adsorption site may be the same as that for As(V).

The arsenic removal of real water sample which contains many competitive ion such as SO_4^{2-}, CO_3^{2-}, SiO_4^{2-}, PO_4^{3-} and humic acid by Mn–Fe binary oxide adsorbents have been reported by literatures.[15,27] Phosphate whose molecular structure is very similar to arsenic ion was the greatest competitor with arsenic for adsorptive sites on the adsorbent. The adsorbent follows the selectivity pattern $PO_4^{3-} > SiO_4^{2-} > CO_3^{2-} > SO_4^{2-}$ and the sulfate and humic acid have no significant effect on arsenic removal.

Conclusions

Mn–Fe binary oxides prepared by alkaline hydrolysis of a mixed solution of $Mn(NO_3)_3$ and $Fe_2(NO_3)_3$ show good adsorption ability for both As(III) and As(V) in a diluted solution. The binary oxide with amorphous or low-crystalline phases exhibits the high arsenic removal ability due to its large surface area. MF4/6-10(H_2O_2) with a mixture of β-MnOOH and amorphous iron hydroxide exhibits the most excellent As(III) removal of 99.9% at pH < 7.5, reducing As(III) concentration to 2 μg L^{-1}, which clears the arsenic limit of 10 μg L^{-1} in drinking water by the WHO. Manganese species in the binary oxide accelerates oxidation of As(III) to As(V), which enhances As(III) adsorption ability of the adsorbent. Iron species in the binary oxide has a role to form surface OH groups, which is an important factor for the effective adsorption of As(V) by surface chelating reaction.

Acknowledgements

This study was supported by the Natural Science Foundation of China (No. 21266014), and Grant-in-Aid for Science Research (B) (No. 26289240) from the Japan Society for the Promotion of science.

References

1 D. Mohan and C. U. Pittman Jr, *J. Hazard. Mater.*, 2007, **142**, 1.
2 X. C. Le, S. Yalcin and M. S. Ma, *Environ. Sci. Technol.*, 2000, **34**, 2342.
3 W. R. Cullen and K. J. Reimer, *Chem. Rev.*, 1989, **89**, 713.
4 P. L. Smedley and D. G. Kinniburgh, *Appl. Geochem.*, 2002, **17**, 517.
5 J. F. Ferguson and J. Gavis, *Water Res.*, 1972, **6**, 1259.
6 W. R. Penrose, *CRC Crit. Rev. Environ. Control*, 1974, **4**, 465.
7 L. G. Roberts, S. J. Hug, T. Ruettimann, A. W. Khan and M. T. Rahman, *Environ. Sci. Technol.*, 2004, **38**, 307.
8 D. R. Borum and C. O. Abernathy, in *Arsenic exposure and health effects, Science and Technology Letter*, Nothwood, U. K., 1994, p. 21.
9 S. Goldberg and R. Johnston, *J. Colloid Interface Sci.*, 2001, **234**, 204.
10 T. R. Holm, *J. Am. Water Works Assoc.*, 2002, **94**, 174.
11 L. S. McNeill and M. Edwards, *J. Am. Water Works Assoc.*, 1997, **89**, 75.
12 J. J. Waypa, M. Elimelech and J. G. Hering, *J. Am. Water Works Assoc.*, 1997, **89**, 102.
13 P. Brandhuber and G. Amy, *Desalination*, 1998, **117**, 1.
14 L. S. Thakur and P. Mondal, *Desalin. Water Treat.*, 2016, 1–17.

15 D. Ociński, I. Jacukowicz-Sobala, P. Mazur, J. Raczyk and E. Kociołek-Balawejder, *Chem. Eng. J.*, 2016, **294**, 210.
16 S. E. O'Relly, D. G. Strawn and D. L. Sparks, *Soil Sci. Soc. Am. J.*, 2001, **6**, 67.
17 L. Dambies, *Sep. Sci. Technol.*, 2004, **39**, 603.
18 P. Mondal, C. B. Majumder and B. Mohanty, *J. Hazard. Mater.*, 2008, **150**, 695.
19 P. Mondal, C. B. Majumder and B. Mohanty, *J. Hazard. Mater.*, 2007, **144**, 420.
20 P. Mondal, B. Mohanty, C. B. Majumder and N. Bhandari, *AIChE J.*, 2009, **55**, 1860.
21 P. Mondal, C. Balomajumder and B. Mohanty, *Clean: Soil, Air, Water*, 2007, **35**, 255.
22 E. A. Deliyanni, D. N. Bakoyannakis, A. I. Zouboulis and K. A. Matis, *Chemosphere*, 2003, **50**, 155.
23 Z. M. Gu, J. Fang and B. L. Deng, *Environ. Sci. Technol.*, 2005, **39**, 3833.
24 Alcan Chemicals, *Product data, AAFS-50*, ALCAN Chemicals, Montreal, Canada, 1998.
25 M. Jang, S. H. Min, T. H. Kim and J. K. Park, *Environ. Sci. Technol.*, 2006, **40**, 1636.
26 D. W. Oscarson, P. M. Huang and U. T. Hammer, *Water, Air, Soil Pollut.*, 1983, **20**, 233.
27 G. S. Zhang, H. J. Liu, J. H. Qu and W. Jefferson, *J. Colloid Interface Sci.*, 2012, **366**, 141.
28 R. Chitrakar, S. Tezuka, A. Sonoda, K. Sakane, K. Ooi and T. Hirotsu, *J. Colloid Interface Sci.*, 2006, **298**, 602.
29 R. Chitrakar, S. Tezuka, A. Sonoda, K. Sakane and T. Hirotsu, *Ind. Eng. Chem. Res.*, 2009, **48**, 2107.
30 J.-Y. Yu, M. Park and J. Kim, *Geochem. J.*, 2002, **36**, 119.
31 S. Saracoglu, M. Soylak and L. Elci, *Acta Chim. Slov.*, 2003, **50**, 807.
32 S. Dixit and J. G. Hering, *Environ. Sci. Technol.*, 2003, **37**, 4182.
33 G. S. Zhang, J. Y. Qi and H. N. Li, *Bioresour. Technol.*, 2015, **193**, 273.
34 Z. Gu, J. Fang and B. L. Deng, *Environ. Sci. Technol.*, 2005, **39**, 3833.
35 G. S. Zhang, J. H. Qu, H. J. Liu, R. P. Liu and R. C. Wu, *Water Res.*, 2007, **41**, 1921.
36 I. Jacukowicz-Sobala, D. Ocinski and E. Kociolek-Balawejder, *Ind. Eng. Chem. Res.*, 2013, **52**, 6453.
37 P. J. Swedlund and J. G. Webster, *Water Res.*, 1999, **33**, 3413.
38 G. S. Zhang, F. D. Liu, H. J. Liu, J. H. Qu and R. P. Liu, *Environ. Sci. Technol.*, 2014, **48**, 10316.
39 H. W. Nesbitt, G. W. Canning and G. M. Bancroft, *Geochim. Cosmochim. Acta*, 1998, **62**, 2097.
40 J. N. Moore, J. R. Walker and T. H. Hayes, *Water Res.*, 2007, **41**, 1921.